Experimental model for study of electro-magnetic phenomena in stator core-end laminations of large generators

Gilles Vogt, Cristian Demian, Raphael Romary, Guillaume Parent, Valentin Costan

Progress In Electromagnetics Research B, Vol. 56, 89–107, 2013

EXPERIMENTAL MODEL FOR STUDY OF ELECTROMAGNETIC PHENOMENA IN STATOR CORE-END LAMINATIONS OF LARGE GENERATORS

Gilles Vogt[1, 2, 3], Cristian Demian[2, 3], Raphael Romary[2, 3, *], Guillaume Parent[2, 3], and Valentin Costan[1]

[1]Electricité de France (EDF) R&D, Clamart 92141, France

[2]University Lille Nord de France, Lille F-59000, France

[3]UArtois, Laboratoire Systèmes Electrotechniques et Environnement (LSEE), Béthune F-62400, France

Abstract—This paper describes an experimental model for the characterization of electromagnetic phenomena that occur within the end regions of large turbo-generators. The study is based on a test bench that contains a stack of steel laminations from a 900 MW turbo-generator stator and two exciting circuits in order to combine a transverse magnetic flux with the in-plane flux. In order to explain the flux penetration within the magnetic sheet stack, accurate experimental measurements are performed. Results are compared with finite-element simulations using *code_Carmel3D*. In the same time, theoretical and experimental results are analyzed with a view to examining the influence of transverse flux on additional losses.

1. INTRODUCTION

Stator magnetic circuits of large turbo-generators in electrical power-plants are subject to electrical, thermal and vibratory stresses, which cause aging and deterioration. Especially, the stator front ends are severely stressed due to the presence of the stray magnetic field induced by the currents in the end windings and in the rotating end connections of the rotor. Indeed, this magnetic field has an axial component which penetrates perpendicularly in the front part laminations. This transverse magnetic field induces in-plane eddy currents in the first

Received 21 August 2013, Accepted 16 October 2013, Scheduled 24 October 2013

* Corresponding author: Raphael Romary (raphael.romary@univ-artois.fr).

laminations, leading to extra losses and overheating. The thermal stress causes fast aging of insulation between laminations at the end-parts of the stator. An insulation breakdown can occur, thus generating stator core faults [1].

The electromagnetic field in these parts of the machine is fully three-dimensional. Until now, finite-element simulations used to compute the magnetic field are mainly based on two-dimensional models [2] or simplified 3D models. These models do not allow the computation of eddy currents or they are based on simplified geometry [3–5]. Moreover, experimental analyses are not easy to implement because they require an experimental bench that represents a real stator or at least a piece of a real stator, what is rather unusual.

This paper presents an analysis based on an experimental apparatus that contains stator laminations of a large turbo-generator.

In our new experimental device, a stator tooth is excited by two incoming fluxes: the main flux (in-plane flux), flowing within the lamination plane; and a transverse magnetic flux, that is perpendicular to the lamination plane.

Both fields can be adjusted separately in amplitude and in phase, so the behavior of the laminations with regard to active and reactive powers of large generators can be reproduced.

This study reports experimental analysis of transverse flux effects and finite element simulation results. The finite element simulation is based on a 3D time-step dynamic model. The stator laminations are modeled by a homogeneous block with isotropic non-linear permeability and anisotropic conductivity. The effects of the transverse magnetic flux will be studied in terms of additional iron losses for a given in-plane flux. Two main results are presented in this paper:

- transverse flux penetration within the stack of laminations, regarding the influence of the saturation induced by the in-plane flux,
- evolution of the losses in the stator tooth with regard to the incoming transverse flux density.

2. OBJECTIVES AND DESIGN

2.1. Background and Objectives

In the end-region of large turbo-generators, the resulting magnetic field has an axial component which comes mainly from the air-gap fringing across the core-end and from the stator and rotor end-winding currents [6]. The effects of the axial-flux can be reduced by introducing a stepped core-end (see Figure 1), a core-end flux shield or by slit cuts

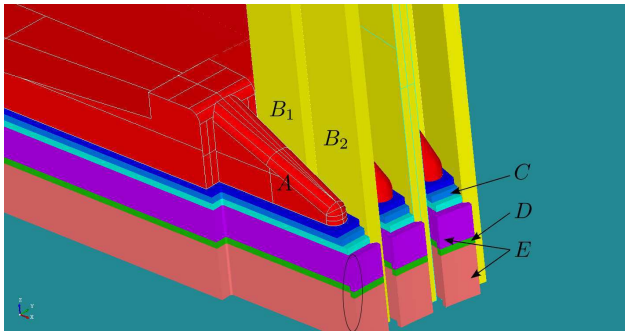

Figure 1. Model of the end-region of the 125 MW turbo-generator stator core, as an example of a stepped core. Zoom on the first steps around the stator teeth (only half a segment is drawn). It is a not-shielded stator, and its fingers are drawn in red (A), the stator bars in yellow (B_1 and B_2), the stepped core-end in shaded blues (C), the cooling ducts in green (D) and the full segments in purple and pink (E) that comprise notches (circled in the figure).

on the stator tooth. However, it still induces high eddy currents and inter-lamination voltages in stator packets [7]. These effects might damage the stator core by breaking down the insulation layer between laminations and thus providing a closed path for a fault current.

Eddy currents induced by the axial flux definitely increase the global stray losses, and hot points are indeed localized in some areas, e.g., the corners at the bottom of stator slots [8]. Both experiments and simulations are thus important to identify the critical areas. The operating conditions also have a major influence on the magnitude of axial flux: it is well known that during leading power factor operations, the temperature rise may be critical and the worst case remains the pole-slip [9].

Experimental measurements are performed on the stator core-end of some large turbo-generators [10, 11], but instrumenting a real turbo-generator remains complicated, and monitoring at operating conditions is usually not possible. These difficulties motivate the use of simulations and simplified experimental devices.

The experimental device designed in the present paper aims at studying the behavior of the magnetic flux in the end-regions of turbo-generators. This study focuses on the combination of fluxes within the stator tooth part and induced losses. Losses are analyzed as function of stator tooth magnetic flux density that imposes the level of saturation.

2.2. Specifications

The experimental device aims at reproducing the behavior of the fluxes in the end-regions of large turbo-generators; thus, it must combine two incoming fluxes. The first one is the "main" flux of the turbo-generator, circulating within the plane of laminations, and the second one is the leakage flux, incoming across the sheets of the magnetic core.

The specifications of the device are therefore:

- Being a good approximation of the phenomena that occur in the end-regions of large turbo-generators;
- Generating a high magnetic flux in the stator tooth (in order to reach the highest saturation level). This flux circulates in the plane of laminations and will be called hereafter the "lengthwise flux";
- Generating a magnetic flux perpendicular to the stator tooth, called "transverse flux";
- Controlling the phase shift between both fluxes in order to reproduce the operating conditions (i.e., lagging/leading mode);
- Measuring the flux penetration inside the stator sheets stack, and measuring losses as function of phase shift between incoming fluxes.

2.3. Design

The final design is depicted in Figure 2. Several choices have been made in order to fulfill above specifications.

2.3.1. Test Core Sheets ((C) in Figure 2)

The chosen testing sample is a part of the stator core of a 900 MW turbo-generator (real scale) limited to one tooth. On the 900 MW turbo-generator, the stator magnetic core is made up of stacked laminations; each layer is divided into 18 segments of three teeth (the stator has 54 slots). The butt joins between laminations are staggered from layers to layers; the shift angle between adjacent laminations is equivalent to one tooth. That is why the angular aperture of one-sample sheet equates to be one third of the actual segments (i.e., one tooth only). A stack of full segments without staggering would not be more accurate.

Besides to focus the lengthwise flux into one single tooth, this design allows increasing the flux density in the stator tooth. Using a full three-tooth segment instead of single tooth would neither improve

the accuracy since the two adjacent teeth would not carry any magnetic flux (unlike what actually occurs).

Moreover, in the end-region of turbo-generators, the stator teeth are shortened (in order to obtain a stepped core-end as shown in Figure 1), thus the notches used to maintain the wedges in this area do not appear in the presented device. Finally, some teeth are designed with slits cut in the radial direction, but this is neglected in the current study. The samples may include this in further studies.

The 900 MW testing sample core (C) is divided into two stacks of laminations: the upper stack contains 56 sheets and the lower stack 88 sheets. The stacks are separated by one epoxy plate of comparable thickness in order to have the effect (in terms of equivalent reluctance) of the air duct present in the real turbo-generator.

The sample sheets are made of grain oriented electrical steel (thickness 0.35 mm). The direction of lamination is crosswise to the tooth.

2.3.2. Exciter Frame ((A) in Figure 2)

The lengthwise flux, which flows within the plane of laminations, is generated by two windings wound on a symmetric exciter frame, as shown in Figure 2. These two windings (B) operate in phase, producing two symmetric fluxes that move back through the stator tooth. However, an asymmetric operation mode would be easy to implement afterward.

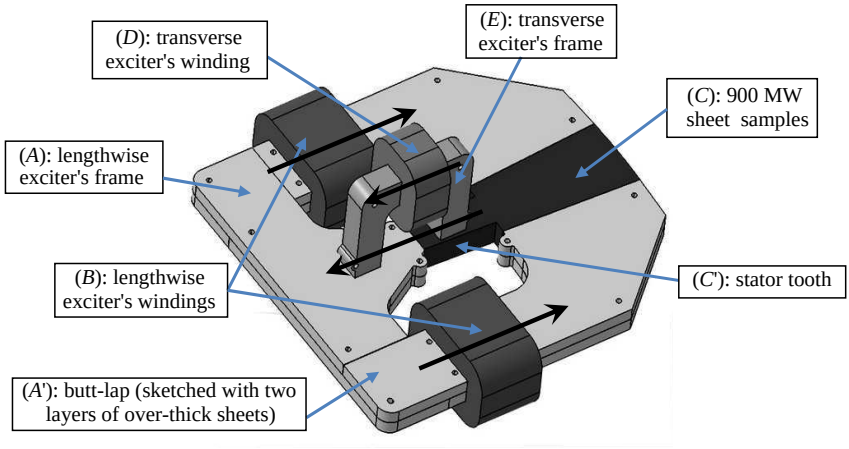

Figure 2. Final design of experimental device with the most important components.

The transverse flux is generated by a second frame in "U" shape (E). It is a mobile frame, so the incoming area on the tooth can be changed. The air-gaps between the exciter frame (A) and the sample core (C) may be adjusted in order to fine-tune the global reluctance of the exciter. The positive directions of the various fields are illustrated in the Figure 2 (i.e., the flux direction when the currents through the exciting winding are in phase).

The frames themselves ((A) and (E)) are made of a stack of 180 laminations (M270-0.35). The lengthwise frame (A) is divided into three parts with butt-lap to reduce the equivalent reluctance of the frame. The transverse (E) frame is made of single part.

2.3.3. Phase Shift between Fluxes

An asynchronous machine with a wound rotor is used as transformer to feed the transverse winding. Therefore, the phase angle between lengthwise and transverse fluxes depends directly on the angular position of the rotor (which is fixed and adjusted using a worm screw).

2.3.4. Windings Sizing

The number of turns must be determined beforehand: the required current to impose a flux decreases when the number of turns increases, thus rising the required voltage. Depending on the chosen power supply characteristics, the best compromise voltage/current must be evaluated. For this, a model based on a reluctance network is used.

2.3.5. Reluctance Network

A simple (linear) reluctance network has been drawn, as shown in Figure 3. The two branches (α) and (α') modeling the lengthwise

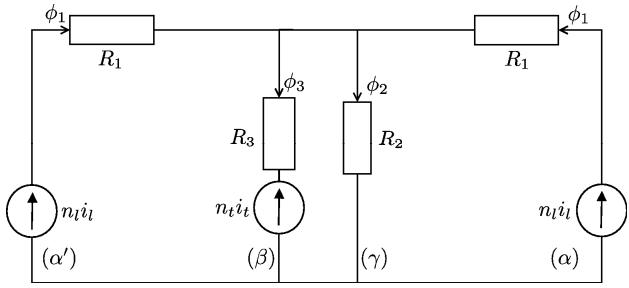

Figure 3. Reluctance network. (α) and (α'): lengthwise frame and windings; (β): transverse frame and winding; (γ): central branch including the tooth.

frame (A) are symmetric: they consist of one magnetomotive force $n_l i_l$ (M.M.F. that represents the winding) and one reluctance R_1. This reluctance R_1 includes the reluctances of the magnetic frame, the butt-lap joint (which equates to an air gap of 0.1 mm [12]), the long air-gap and a part of the sample (depending on the position of the transverse frame). The branch (β) corresponds to the transverse frame: the M.M.F. $n_t i_t$ and the reluctance R_3 that includes the reluctance of two air-gaps and magnetic frame reluctance. Finally, the branch (γ) (reluctance R_2) represents one part of the sample core (complementary to the α's part), tooth air-gap and the part of the lengthwise frame that faces the tooth (triangular-shaped).

The saturation of the material is taken into account through the adaptation of the magnetic permeability. In the areas where the flux density is expected to be high (confirmed by FEM simulation), such as the stator tooth, the permeability is lowered. The relative permeability of the lengthwise frame is 4000, while the tooth's one is only 500 (which is coherent with a flux density of 1.7 T).

The reluctance of a circuit $[AB]$ (where AB is an arbitrary flux path) is calculated using Equation (1), where l is the curvilinear abscissa, S and μ the cross section and permeability:

$$R = \int_A^B \frac{dl}{\mu(l) \cdot S(l)} \tag{1}$$

Of course, in the case where the permeability and section are constant, the formula becomes $R = l_{AB}\mu \cdot S$.

This leads to the electrical equations that describe the behavior of the system. The results are shown in Table 1 which points out that the exciter frames provide an alternative path for the flux. Adjusting the air-gaps accordingly (e.g., by increasing the transverse air-gaps) will allow one to control this path. Nevertheless, the reluctance network highlighted this intrinsic restriction of the device.

Table 1. Reluctances of the main parts of the device (*cf.* Figure 3).

Portion	Value (H^{-1})
Tooth (total)	$10.6 \cdot 10^4$
Tooth air-gap	$2.1 \cdot 10^4$
Long air-gap	$2.1 \cdot 10^4$
Transverse air-gap	$3.2 \cdot 10^4$
Transverse frame	$4.2 \cdot 10^4$
Lengthwise frame	$2.2 \cdot 10^4$

Reluctance	Value (H^{-1})
R_1	$18.1 \cdot 10^4$
R_2	$6.7 \cdot 10^4$
R_3	$11.6 \cdot 10^4$

The lengthwise windings are sized by shutting down the transverse winding supply, and *vice versa*. For instance, the global magnetic equation for the lengthwise case is:

$$\phi_2 \left(R_2 + \frac{R_2 + R_3}{2R_3} R_1 \right) = n_l i_l \tag{2}$$

where n_l is the number of turns and i_l the current in the lengthwise windings. In order to gauge the number of turns, a flux density set-point B_{obj} in the tooth is chosen, leading to the system (4).

$$e_l = -n \frac{\partial \phi_l}{\partial t} = -n \frac{\partial \int_{S_l} \vec{B}_{obj} \cdot \vec{dS}}{\partial t} \tag{3}$$

where e_l is the voltage at the terminals of the lengthwise windings and ϕ_l the magnetic flux through the windings section. Considering the dimension of the device and the values given in Table 1, the Equations (2) and (3) lead to:

$$\begin{cases} i_l = \frac{1}{n_l} \cdot 629 \cdot B_{obj} \\ e_l = 0.94 \cdot n_l \cdot B_{obj} \end{cases} \tag{4}$$

The flux density objective level B_{obj} is set to 1.7 T and it appears that $e_l = 240\,\mathrm{V}$ and $i_l = 7\,\mathrm{A}$ (for each winding) are enough with $n_l = 150$ turns. The same analysis (with $B_{obj} = 1\,\mathrm{T}$) for the transverse exciter leads to the same number of turns ($n_t = 150$), but with much lower electric levels ($i_t = 5\,\mathrm{A}$ and $e_t = 140\,\mathrm{V}$).

3. EXPERIMENTAL RESULTS

3.1. Instrumentation and Measurement Protocol

Our experimental device has been instrumented in order to study the magnetic behavior of the sample core excited by two incident fluxes. Firstly, search coils have been implemented to measure the flux actually flowing in the iron near to the windings (B) and (D) and through the end of the tooth (C'), as shown in Figure 2. Secondly, in order to measure the penetration of the magnetic flux in the transversal direction to the magnetic sheets ((C') in Figure 2), about 15 flat search coils have been placed within the first and the second stack of laminations. The measurements are simultaneously picked up thanks to a Labview data acquisition system. The losses are measured with a precision wattmeter while fluxes are computed from search coil voltage waveforms. The use of search coils allows to subtract the losses from Joule effect induced in windings (B) and (D). Before each measurement sequence, the device is powered for several minutes to avoid the possible drift due to temperature variation.

3.2. Penetration of Magnetic Field

In order to analyze the behavior of the magnetic flux when it incomes perpendicularly to the plane of laminations, several studies have been carried out. The first one focuses on the penetration of the transverse magnetic flux in the stack of laminations and determines the influence of the tooth magnetic state. The results presented in Figure 4 illustrate the perpendicular magnetic flux density measured by the flat search coils placed inside the laminated stack considering three magnetic states of the stator tooth:

- non excited tooth (i.e., lengthwise exciters short-circuited),
- tooth excited at 1.5 T,
- tooth excited at 1.8 T (saturated tooth).

In the two last cases, the lengthwise flux naturally flows through the transverse frame. Then, the resulting transverse flux is adjusted (increased or reduced) by modifying the currents in the transverse winding. Currents are adjusted in order to bring the resulting flux density at 1.5 T and 1.8 T in the tooth.

From Figure 4, it can be observed that the magnetic flux density in the tooth is gradually affected according to its magnetic state. In the case of saturated tooth (1.8 T), the slope of the attenuation is relatively constant; the flux goes into the depth of the first stack of laminations, flows through the air cooling duct and penetrates into the next stack of laminations at about 50 mT. When the tooth is not saturated, the

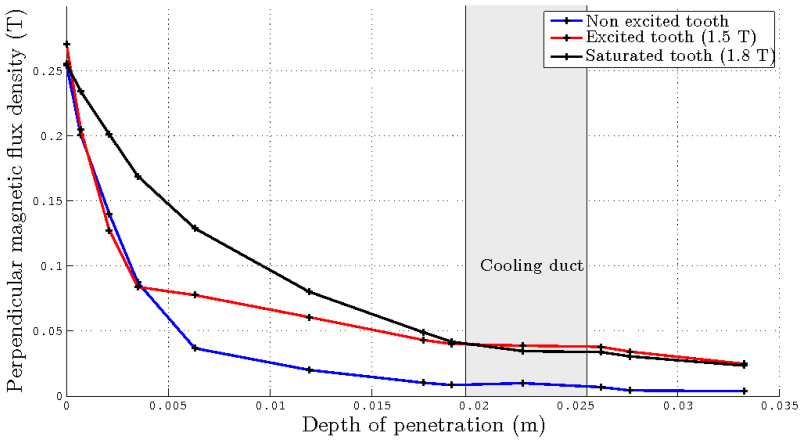

Figure 4. Effect of the tooth saturation on the depth of the perpendicular magnetic flux penetration.

flux is rapidly attenuated and become negligible in the second stack of laminations. For the same incident flux density (around 250 mT), the flux density in the air duct is five times higher (50 mT/10 mT) when the tooth is saturated by the lengthwise excitation.

3.3. Loss Measurement

3.3.1. Influence of the Transverse Frame (Passive)

These experiments aim at analysing the effect of the exciter frame itself, and its consequences on the losses. Both lengthwise windings (B) generate an in-phase flux flowing though the stator tooth (up to 1.8 T). Two cases are considered:

- the transverse frame is absent,
- the transverse frame is placed in the position described in Figure 2, and the transverse winding is in open-circuit.

The overall flux path in the tooth is changed by the presence of the transverse frame. It has been found that around 5–8% of the flux (depending on the tooth saturation) is driven through the transverse frame. This flux is therefore perpendicular to the lamination plane and induces additional losses. The increase of losses is presented in Figure 5.

As the magnetic flux in the lengthwise arm increases, the tooth saturates and the transverse flux rises and flows deeper in the stack. The additional losses generated by the in-plane eddy currents increase. It can be observed from Figure 5 that these additional losses represent 35% of the whole losses at maximum lengthwise flux whereas it falls to some percents for low lengthwise flux.

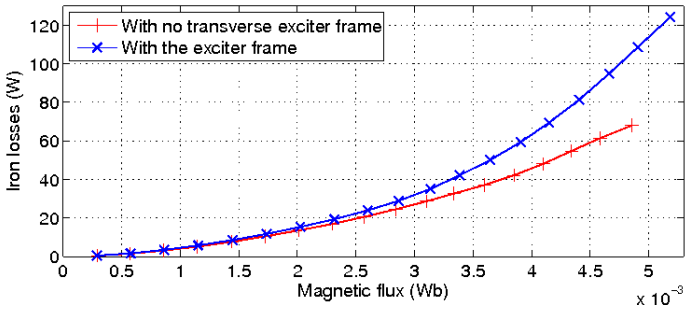

Figure 5. Iron losses seen from one lengthwise winding (B) function of the magnetic flux in one lengthwise arm.

3.3.2. Evaluation of Tooth Losses

In this section, both transverse and lengthwise exciter windings are supplied. The currents in the lengthwise exciters generate 3.8 mWb in each lengthwise arm, and thus saturate the tooth. In order to evaluate the losses in the tooth due to the transverse flux, several experiments are made:

1. The transverse frame is fully on the lengthwise exciter (Figure 6, experiment 1), the lengthwise windings (B) are short-circuited whereas the transverse exciters winding (D) generates a magnetic flux. Eddy currents are induced in two regions located on the lengthwise exciter.
2. The transverse frame is in the position shown in Figure 6, experiment 2. The lengthwise windings induce a high flux (3.8 mWb in each arm) flowing in-phase through the tooth. In-plane eddy-current losses are induced in the tooth and in the lengthwise frame.
3. The transverse frame is absent, and the (B) windings induce the same flux as in experiment 2. There are no in-plane eddy current losses.
4. Same as 2, but in this case, one arm of the transverse frame (E) is situated on a saturated area of the lengthwise exciter (near the tooth). Therefore, in this region, losses will be induced by both lengthwise and transverse fluxes. Eddy current losses are located only in the lengthwise frame.

The losses within the tooth due to the transverse flux corresponding to experiment 4 are therefore:

$$P_T = P_2 - P_3 - \left(P_4 - \frac{1}{2}P_1\right) \tag{5}$$

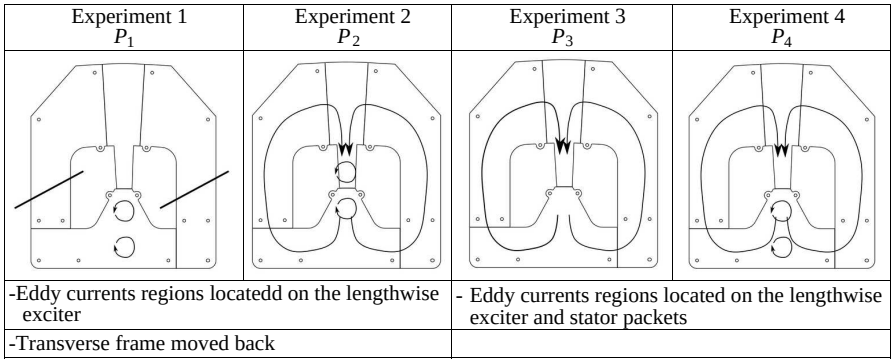

Figure 6. The different positions of the transverse frame.

where P_i are the total losses tied to experiment i excepted in the case of P_4 where only the losses seen from the transverse winding (D) are taken into account.

The additional losses due to the transverse field are presented in Figure 7. The flux flowing through the lengthwise arms remains constant, and the losses due to this lengthwise flux in the whole magnetic circuit are 78 W. Assuming that around half of the losses are localized in the stator tooth, the additional losses under a 0.25 T transverse flux represents an increase of 12% of the losses in the tooth.

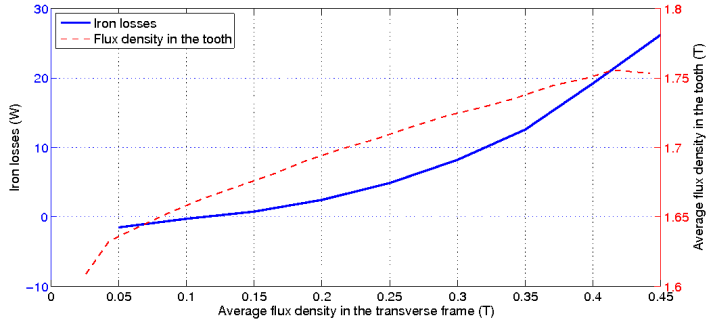

Figure 7. Additional losses in the tooth due to the transverse flux only.

4. FEM SIMULATIONS

The finite element model of the experimental apparatus is used to characterize the flux density distribution inside the stator packets imposing different values of the currents through the exciting circuits.

The FEM (Finite Elements Method) simulations are run with *code_Carmel3D*. This software is based on Whitney's elements and is developed by the LAMEL ("*Laboratoire de Modélisation du Matériel Electrique*", common laboratory between EDF R&D and L2EP).

The simulation is performed using a time-step magneto-dynamic model. The step time is 1.67 ms and the results are exploited once the steady state is reached. All the magnetic parts are considered as an isotropic iron block with a non-linear B(H) curve. Only the tooth is modeled as a conductive material but with anisotropy such that the conductivity is imposed at 500 Sm^{-1} in the transverse direction and $2.08.10^6$ Sm^{-1} in the lengthwise direction. Therefore, the calculated losses originate from in plane-eddy currents only, because the currents in the transverse direction are insignificant.

4.1. Mesh of the Experimental Apparatus

The geometric model is based on the true geometric shape of the experimental model, including screw holes and all details presented in the geometry. By using symmetry of the experimental device, only one half of the magnetic circuit has been modeled. In the critical areas (i.e., the high-gradient areas), the mesh quality has to be controlled: the aspect ratio of tetrahedrons should be as close to 1 as possible in order to improve the FEM simulation robustness. The mesh sizes near the air-gaps are set to depend directly on the corresponding air-gap thickness ε; usually, the characteristic length ranges from 0.5ε to 1.5ε. Since the tooth air-gap is really small compared to the global size of the model (0.1 mm compared to 150 mm), the generated mesh size is acceptable: 1.10^6 tetrahedrons (Figure 8).

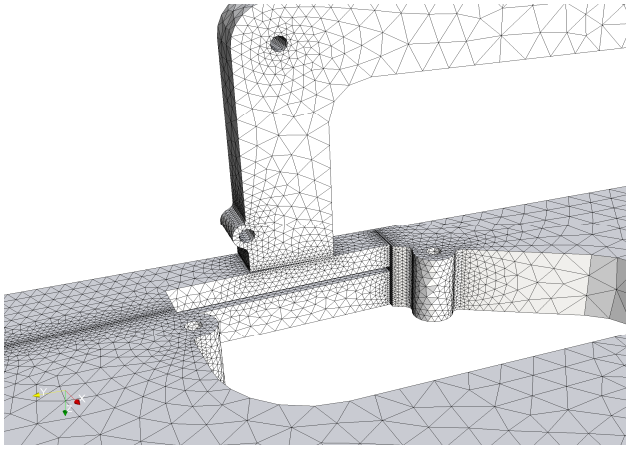

Figure 8. The geometric model mesh.

The mesh is obtained by using the software Gmsh [13] and Salome (Netgen algorithm). It can be noted that packets of laminations are meshed as a homogeneous block (treated as an anisotropic medium), allowing to greatly reduce the mesh size.

4.2. Penetration of Magnetic Field

As done in the experiments, the current flowing through all three windings is set to induce in-phase fluxes through the stator tooth. Three situations are considered:

- non excited tooth, lenghtwise windings are not supplied,

- excited tooth, the excitation is modified to get 1.5 T flux density though the tooth,
- saturated tooth, the currents in the lenghtwise windings allow obtaining up to 1.8 T flux density through the tooth.

In Figure 9, the "trend" curves are plotted from simulation results (continuous lines). Simulation results are illustred in dotted lines. It can be noted that the simulation results present similar tendencies than experimental data, considering the saturated and non excited slot tooth (Figure 4). As expected, when the tooth is saturated, the decay of the transverse flux density is lower and a significant amount of the transverse flux is present in the second stack of laminations. The perpendicular flux in the second stack is about 80 mT. In the case of non excited tooth, the flux density is rapidly attenuated and flows through the first lamination sheets of the upper stack. The lower stack of laminations is not affected: the transverse flux density is about 3 mT.

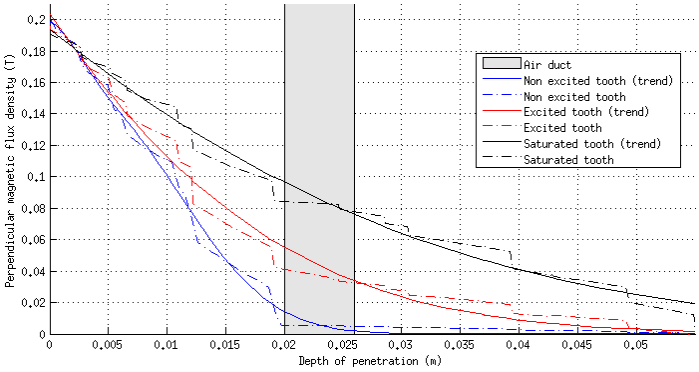

Figure 9. Effect of the tooth saturation on the depth of the perpendicular magnetic flux penetration: FEM simulation.

The trends of the simulation results are coherent, but some differences appear with the experimental results where the slopes are higher. It is mainly due to the magnetic model of the sample core: actually, our software being currently in development, it does not include yet all the features we need, especially the anisotropic non-linear permeability. Indeed, magnetic steel laminations are highly anisotropic (the transverse permeability being really low), and the homogenization of a stack is also per se anisotropic.

This being said, this study produces consistent results (that could be improved), and the simulation time is currently quite low: 3 h/time step in the most complicated cases. Modeling each lamination

individually and the insulation between them could lead to more accurate results only if the anisotropy of each layer is taken into account. However, in this case the mesh would be much heavier, and the needed memory thus much higher.

4.3. Loss Analysis

4.3.1. Loss Density Distribution

Finite element analysis evaluates the distribution of loss density. In a first simulation, the current in the transverse exciter is opposed-phase relatively to the lengthwise one, what leads to induce in-phase

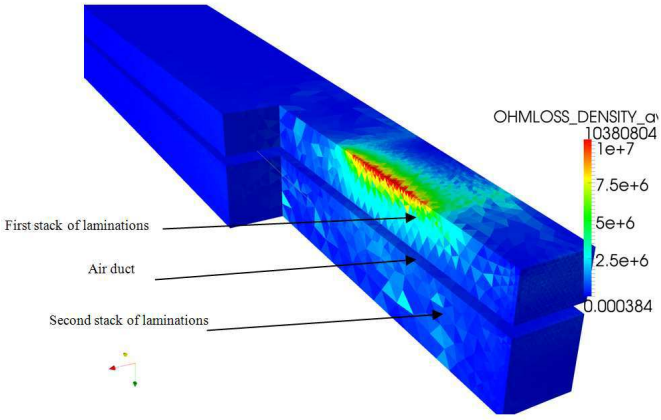

Figure 10. Excited tooth: loss repartition (W/m^3) within the tooth (only half of the device is drawn- the other half is symmetric).

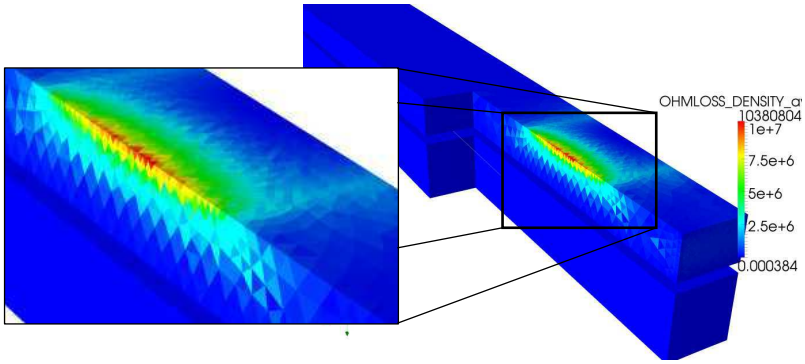

Figure 11. Non excited tooth: loss repartition (W/m^3) within the tooth.

fluxes flowing through the tooth. The currents are set up in order to obtain 1.65 T in the tooth, and 0.4 T for the transverse flux density. The obtained flux density map is illustrated in Figure 10. It can be observed that the loss density is mainly distributed in the first stack of laminations. Figure 11 gives the loss distribution in case of non excited tooth considering the same transverse flux density (only the transverse exciter is supplied). It can be observed that a higher loss density area appears in the top of the sheet stack. These results can be related to the penetration of the transverse flux in the stack of laminations.

4.3.2. Comparison between Simulations and Experimental Losses

The losses calculated by the FEM simulation are accurate compared to the experimental measurements. The comparison is presented in Figure 12: the losses are drawn versus the incoming perpendicular flux. Experimental losses are higher than simulation ones because the hysteresis losses are neglected in this work; however, the correlation is quite good despite the simplifications of the magnetic model.

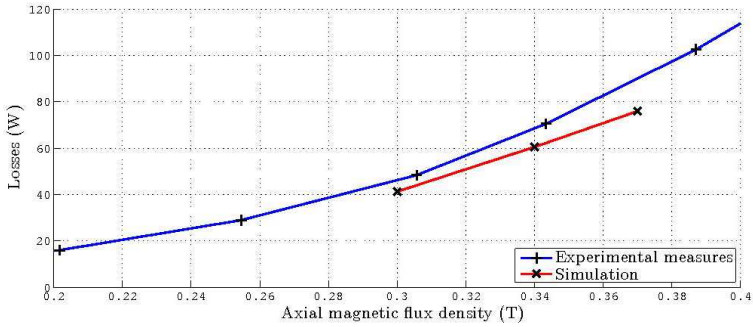

Figure 12. Comparison of simulated and experimental losses.

5. CONCLUSION

The experimental apparatus has been carefully presented: the methodology used for designing the device was explained with respect to background and objectives, in a way intended to be systematic and pedagogic. A simple reluctance network was used to anticipate the global flux behavior (in regard to air-gaps notably) and determine the winding characteristics (number of turns, current, voltage). The experimental model has been instrumented in order to measure the penetration of the transverse flux and to evaluate the losses.

Some results have been presented regarding the effect of the transverse flux on the stator tooth. First, the penetration of the transverse flux in the sheet packet has been investigated. It appears that it strongly depends on the level of saturation. Then, the passive effect of the transverse frame has been analyzed: a small part of the magnetic flux flowing through the tooth is passively deflected by the transverse frame. It has been shown that the transverse flux coming from the flux deviation leads to an important increase of losses. For example, in a real turbo-generator, this deviation embodies the air gap fringing. A second result deals with the increase of losses in the tooth as a function of the amplitude of the incoming transverse flux density. Based on the losses of four experimental setups, we have deducted the losses occurred in the tooth due to the axial flux only.

Finite elements analysis (3D) confirms the tendencies of the experimental results, and it gives a finer idea of the loss repartition in the tooth. However, in order to improve to accuracy of results, an adapted modeling that considers homogenized non-linear anisotropic material should be developed. This model could be validated thanks to the experimental results. Then, the Finite Element analysis could be extended to model the whole end region of a turbo-generator as far as the computational requirements are acceptable.

In the future, more features could be added to the experimental device, such as teeth slits. Asymmetric lengthwise excitations may also be studied. The transverse flux incoming area could be improved by covering a bigger area upon the stator tooth, similarly as in real turbo-generators.

NOMENCLATURE

R — reluctance of a circuit,
l — curvilinear abscissa,
S — current section,
μ — permeability,
M.M.F. — magnetomotive force,
n_l — number of turns,
i_l — current in the lengthwise windings,
e_l — voltage across the lengthwise winding terminals,
ϕ_l — magnetic flux through the winding section,
B_{obj} — flux density objective level,
FEM — finite elements method,
ε — air-gap thickness.

ACKNOWLEDGMENT

This work is supported by MEDEE program supervised by the French national technological research cluster on electrical machine efficiency increase. This program that includes Électricité de France R&D is sponsored by the region Nord Pas-de-Calais (France) and the French ministry and the European founds (FEDER).

REFERENCES

1. Tavner, P. J. and A. F. Anderson, "Core faults in large generators," *IEE Proceedings — Electric Power Applications*, Vol. 152, No. 6, 1427–1439, 2005.
2. Drzymała, P., K. Komeza, H. Welfle, S. Wiak, D. Kardas, and S. Sieradzki, "Field analysis of end regions of stator windings of large turbogenerators," *ISEF 2009 — XIV International Symposium on Electromagnetic Fields in Mechatronics, Electrical and Electronic Engineering*, 2009.
3. Lin, R., A. Haavisto, and A. Arkkio, "Analysis of Eddy-current loss in end shield and frame of a large induction machine," *IEEE Transactions on Magnetics*, Vol. 46, No. 3, 942–948, 2010.
4. Yamazaki, K., S. Tada, H. Mogi, Y. Mishima, C. Kaido, S. Kanao, K. Takahashi, K. Ide, K. Hattori, and A. Nakahara, "Eddy current analysis considering lamination for stator core ends of turbine generators," *IEEE Transactions on Magnetics*, Vol. 44, No. 6, 1502–1505, 2008.
5. Fujita, M., T. Tokumasu, H. Yoda, H. Tsuda, K. Ito, and S. Nagano, "Magnetic field analysis of stator core end region of large turbogenerators," *IEEE Transactions on Magnetics*, Vol. 36, No. 4. 1850–1853, Jul. 2000.
6. Mecrow, B., A. Jack, and C. Cross, "Electromagnetic design of turbogenerator stator end regions," *IEE Proceedings C — Generation, Transmission and Distribution*, Vol. 136, No. 6, 361–372, Nov. 1989.
7. Jackson, R., "Interlamination voltages in large turbogenerators," *Proceedings of the Institution of Electrical Engineers*, Vol. 125, No. 11, 1232–1238, 1978.
8. Lee, S. B., G. Kliman, M. Shah, W. Mall, N. Nair, and R. Lusted, "An advanced technique for detecting inter-laminar stator core faults in large electric machines," *IEEE Transactions on Industry Applications*, Vol. 41, No. 5, 1185–1193, Sep.–Oct. 2005.

9. Singleton, R., P. Marshall, and J. Steel, "Axial magnetic flux in synchronous machines: The effect of operating conditions," *IEEE Transactions on Power Apparatus and Systems*, Vol. 100, No. 3, 1226–1233, 1981.
10. Hilliar, R., R. Jackson, D. Ward, and R. Bennett, "Measurements of the currents flowing in the stator frame of a 500 MW turbogenerator," *IEE Proceedings C — Generation, Transmission and Distribution*, Vol. 133, No. 1, 16–25, 1986.
11. Platt, R., L. Kerr, and A. Anderson, "Measuring flux and interlaminar voltage in turbine generator end regions," *IEE EMDA Conf.*, Vol. 213, 201–205, London, 1982.
12. Karapetoff, V., *The Magnetic Circuit — Electromagnetic Engineering,* M. Books, Ed., Watchmaker Publishing, 2003.
13. Geuzaine, C. and J.-F. Remacle, "GMSH: A 3-D finite element mesh generator with built-in pre- and post-processing facilities," *International Journal for Numerical Methods in Engineering*, Vol. 79, No. 11, 1309–1331, 2009, Online Available: http://doi.wiley.com/10.1002/nme.2579.